Journal of Constructional Steel Research 239 (2026) 110221

Contents lists available at ScienceDirect

Journal of Constructional Steel Research

journal homepage: www.elsevier.com/locate/jcsr

Enhanced Radial Stress Method (RSM) for cellular beams in EN 1993-1-13 to account for elasto-plastic behaviour

Georgios Psyrras [a], Konstantinos Daniel Tsavdaridis [a,*], R. Mark Lawson [a,b]

[a] Department of Engineering, School of Science & Technology, City St George's, University of London, Northampton Square, EC1V 0HB London, UK
[b] The Steel Construction Institute, Unit 2, The E Centre, Bracknell RG12 1NF, UK

ARTICLE INFO

Keywords:
Vierendeel bending
Elasto-plastic behaviour
Plastic hinges
Yield load
Radial stress method
Finite element analysis

ABSTRACT

In cellular beams with circular openings, *Vierendeel* bending failure is caused by the local bending around the web openings in regions of high shear. In BS EN 1993-1-13, a Radial Stress Method (RSM) is presented, which is based either on the elastic resistance of the inclined T-sections around the openings or on their plastic bending resistance dependent on the section classification of the inclined T-section, which results in a step between elastic and plastic properties. The RSM method also fails to account for stress redistribution between the lower moment side and the higher moment side of openings. This study investigates the RSM for circular openings in a typical UB 457x152x52 beam, that is modelled and analysed using Abaqus. The RSM is extended to an elasto-plastic analysis of the inclined T-sections that gives a way of evaluating the development of the *Vierendeel* bending mechanism and may be used for slender webs. The elasto-plastic analysis around the openings subject to axial force, shear and bending is based on a multiple of the yield strain at the edge of the opening. This is compared to the non-linear FEA results, which show good agreement for the stress distribution around the openings on the lower moment and higher moment sides of the openings for all combinations of applied shear and moment. The results of the method are also compared to cellular beam tests results failing in Vierendeel bending.

1. Introduction

The *Vierendeel* bending mechanism occurs when the bending resistance of the web-flange T-sections is reached at four locations around the web openings in regions of high shear, as shown in Fig. 1. This mode of failure was first reported by Altifillisch et al. [1] for castellated beams, and Redwood and McCutcheon [2] for cellular beams.

For a perforated steel beam subject to shear, the Tee sections above and below the web openings resist the applied shear, as well as the primary and secondary stresses in the reduced depth section. The primary stress is caused by the global bending moment acting on the beam. The secondary stresses, also known as *Vierendeel* bending stresses, result from the action of the shear force over the horizontal equivalent length of the opening, which introduces secondary moments in the Tees.

This is the most dominant failure mode for a perforated beam where the interaction between the web openings is negligible. For closely-spaced openings, web-post shear or buckling resistance can govern the behaviour of the beam and so the centre to centre spacing of the openings should generally exceed the beam depth to avoid this failure mode. This study focusses on the *Vierendeel* bending resistance of single openings.

For rectangular and hexagonal web openings, the 'plastic' hinges are formed at the corners of the openings due to the stress concentrations in those locations, but in circular web openings determining the location of the highest stresses is not as straightforward as it depends on the shear-moment ratio acting at the opening.

Early work on cellular beams, carried out by Redwood [4], showed that a circular web opening could be treated as an equivalent rectangular web opening for Vierendeel bending, in which the effective length of the opening is taken as $0.45h_o$ (where h_o is the opening diameter) and its depth as $0.9h_o$ diameter. This approach, referred to as 'Equivalent Rectangular Opening Method', provides a simple way to determine the *Vierendeel* bending moments. This method is a simplification of the shear transfer across circular openings [3], which is useful for 'hand calculations'.

Alternative methods were developed by Olander [5] and Sahmel [6] for elastic stress analysis around circular openings based on the equilibrium of forces on radial cross-sections at increments of the radial angle. Those methods are known as 'curved beam theories' and they were based on the 'wedge method', originally proposed by Osgood [7].

* Corresponding author.
E-mail address: konstantinos.tsavdaridis@city.ac.uk (K.D. Tsavdaridis).

https://doi.org/10.1016/j.jcsr.2025.110221
Received 9 October 2025; Received in revised form 10 December 2025; Accepted 27 December 2025
Available online 5 January 2026

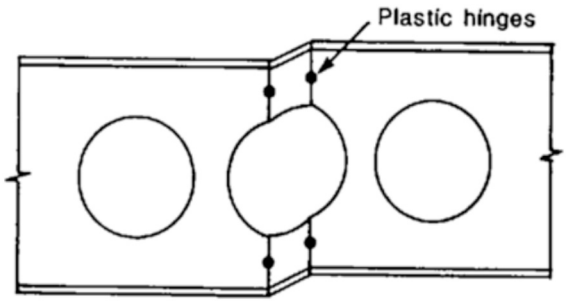

Fig. 1. Vierendeel bending mechanism in the perforated cellular beam section (Ward [3]).

Another analytical method was developed by Blodgett [8] for the analysis of elastic stresses in castellated beams.

Yost et al. [9] demonstrated how Blodgett's method can be used for cellular beam sections with circular openings. The critical angle and the critical stress around the openings were compared to the experimental and FEA results of cellular beams under elastic conditions, which showed good agreement between Blodgett's analysis and the experimentally measured stresses.

Lawson et al. [10] used a method based on equilibrium of forces acting on radial planes at an angle θ relative to the vertical centreline of the web opening, which also takes into consideration the intercepting radial planes from adjacent web openings. It was tested on stainless steel cold formed beams with both widely and closely spaced openings and was compared to experimental and FE test results. The critical angle of the highest radial stresses occurs at an angle of 25 to 35° to the vertical depending on the ratio of the opening diameter to the beam depth, h_o/h.

In BS EN 1993-1-13 [11], the methodology to determine the *Vierendeel* bending resistance of various opening shapes is based on the definition of an equivalent rectangular opening in which the use of elastic or plastic bending resistance of the web-flange T-sections of the equivalent rectangle is dependent on the section classification of the web and flange outstands. An alternative radial stress method is presented for circular openings which is more accurate but more complex to use and it also uses the same section classification method as for an equivalent rectangle. In both methods, this means there is a step between the use of elastic and plastic resistances, and the plastic bending resistance of a T-section can be twice its elastic bending resistance. This is a deficiency in the methodology in BS EN 1993-1-13 which this paper addresses by introducing a gradual transition from elastic to plastic bending resistance in the radial stress method as a function of the edge strain around the openings.

Also, after initial yielding, there is significant redistribution of stresses between the lower and higher moment sides of the opening, which leads to higher load carrying capacity. Chung et al. [12] observed that not all four high stress concentrations result in plastic hinge formation, and that the fully plastic hinges may appear in different locations than those indicated by the onset of yielding.

Chung et al. [13] proposed a design method based on generalised shear-moment interaction curves. The interaction curves were formed from FE results, after conducting nonlinear analyses on typical UB beams with a single circular web opening of varying size. This design method was also employed in [14].

Tsavdaridis and D'Mello [15,16] included six standard and five non-standard web opening shapes, placed on various positions along typical UB beams in order to introduce different shear-moment actions on its vertical centreline.

Panedpojaman et al. [17] proposed a simplified design method, applicable to steel beams with circular or elongated circular openings, which accounts for the interaction of the shear force, the axial force and the *Vierendeel* bending moment on the cross-section.

The current research work aims to provide an improved understanding of the *Vierendeel* bending failure mechanism in steel beams with circular web openings, and to present a novel analysis method that can model the beam's elasto-plastic behaviour. This is based on an extension of the Radial Stress Method (RSM) to determine the elasto-plastic bending resistance of the inclined Tee sections at incremental angles around the higher and lower moment sides of the openings, which are alternately in tension and compression at the edges of the opening. The proposed method allows for the determination of the shear force corresponding to any level of plasticity in the reduced web section, and vice versa. Furthermore, it captures the stress redistribution between the lower and higher moment sides, which is important in design for Vierendeel bending. These significant enhancements address the limitations of the original RSM, which is constrained to an either elastic or purely plastic stress analysis. The elastic and elasto-plastic RSM results are compared to finite element results for 4 openings with constant shear but variable global bending moments to determine the effect of the moment and shear ratios at the openings. The methodology applies to openings without interaction between closely spaced openings.

Other shapes of web openings include rectangular, hexagonal, elongated circular and elliptical openings. The *Vierendeel* bending resistances of rectangular and hexagonal openings are determined at the end of the horizontal part of the opening, which can be analysed using the elasto-plastic properties of the T-sections. Lawson et al. [18] presented tests on cold formed C section beams with elongated openings and showed how the RSM may be adapted by increasing the moment on the radial plane as a result of the elongated part of the opening. This was limited to elastic design for Class 4 sections and therefore the application of elasto-plastic properties to elongated circular openings is outside the scope of this paper.

In composite cellular beams, the compression force in the top Tee is reduced due to composite action with the concrete slab and so the stresses around the opening are also reduced. However, the method in this paper may be applied conservatively to composite beams.

2. Examination of the *Vierendeel* mechanism using non-linear FEA

For this study, a UB 457x152x52 beam in S355 steel with circular openings of diameter h_o = 337 mm (75 % of the section height) was analysed. Studies found in the literature [13,14] showed that the thin web (t_w = 7.6 mm) of this section profile with a web depth to thickness ratio of $70t_w\varepsilon$ is not susceptible to buckling around the opening, ensuring that the formation of the characteristic *Vierendeel* mechanism would occur.

The centre-to-centre distance between adjacent openings was taken as s = 500 mm (i.e. s = 1.48h_o), which was not expected to result in web-post failure. The end-post width s_e was taken as equal to the web-post width s_o (=163 mm). The beam was subject to constant shear force applied at one end of the modelled half-span of 0.5 L = 2081 mm. The equivalent span: depth ratio of 9.2 for this point loaded beam implies that shear rather than bending will control the beam design. The beam's geometry is provided in Table 1.

2.1. Finite element modelling

The finite element analysis software Abaqus CAE [19] was used for this study. For computational efficiency, 'XSYM' boundary conditions

Table 1
Geometric properties of the perforated UB 457×152×52 modelled as a half span beam.

h	b_f	t_f	t_w	h_o	s	$s_o = s_e$	0.5 L
449.8 mm	152.4 mm	10.2 mm	7.6 mm	337 mm	500 mm	163 mm	2081 mm

[20] were applied at the beam's midspan so that only half of the beam was modelled (Fig. 3).

To mesh the geometry, 3D planar shell elements were used, a combination of 4-node (S4R) and 3-node (S3) reduced integration shell elements. A mesh sensitivity study was conducted by comparing the results of four global mesh sizes (20 mm, 15 mm, 10 mm, 5 mm) in terms of applied shear force versus mid-span deflection and stress contours. The global seed size of 10 mm ensured that the solution converged and therefore was selected as it provided the optimal balance between computational efficiency and accuracy. Around the circular openings, a more detailed mapped meshing was used (Fig. 3); the circumference of each opening was discretised into 360 equal-sized elements edges, corresponding to a 1° increment. This specific refinement was essential to place a mesh node at every degree, enabling the direct extraction of nodal stresses for a precise comparison with the analytical results (see Section 3.3). In this way, accurate stress results were obtained for each increment of the radial plane angle θ, without the need of interpolating results between neighbouring nodes.

A generic quad-linear material law, proposed by Yun and Gardner [21], was used for modelling the S355 steel grade, which includes a yield plateau and takes into consideration the strain-hardening behaviour. The stress-strain curve is shown in Fig. 2, and the properties of this material law are given in Table 2.

A point load applied at mid-span was used because a constant shear force along the beam makes the comparison between the behaviour of the web openings with varying global moment more straightforward. First failure by Vierendeel bending was expected to occur at the opening nearest to mid-span, where the bending moment is the highest.

Lateral restraints to the flanges were applied between adjacent openings to ensure that out-of-plane movement of the beam would not occur. These restraints were placed in locations that would not affect the stress distribution in the vicinity of the web opening (Fig. 3).

A geometrically and materially non-linear static analysis with imperfections (GMNIA) was conducted using the Riks method of Abaqus Standard Solver. For this type of analysis, a reference load is used to represent the point load, and the actual load magnitude is received on the analysis completion.

Kinematic coupling constraints were used on both sides of the symmetric beam; on the pinned support side the coupling constraint ensured that there would not be any rigidity at the support, allowing the beam to rotate freely, while at mid-span the constraint distributed the applied point load uniformly as a shear force over the entire cross-section.

In addition to the beam with the four openings, four more beams with single-openings of identical dimensions (Fig. 4) were modelled and analysed in order to study the stress distribution around the isolated web openings and assess the effect of the stress interaction between adjacent web openings.

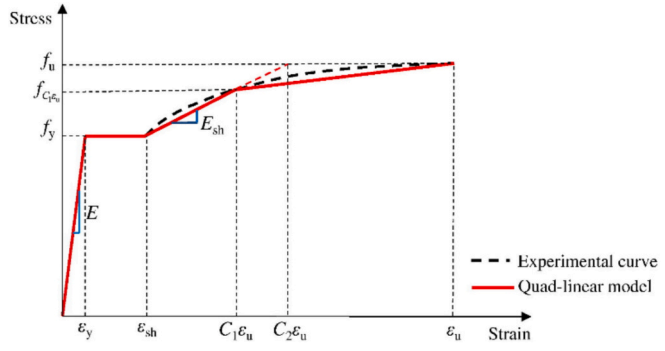

Fig. 2. Standardised quad-linear material law for generic use (Yun and Gardner [21]).

Table 2
Properties of the quad-linear material law for S355 nominal steel grade.

E	f_y	f_{c1eu}	f_u	ε_y	ε_{sh}	$c_1\varepsilon_u$	ε_u
210 GPa	355 MPa	440 MPa	490 MPa	0.0017	0.0174	0.055	0.1653

2.2. Finite element analysis results

The four-opening cellular beam failed by *Vierendeel* bending at the opening closest to mid-span, where the primary bending moment is highest. The applied load versus the mid-span vertical displacement curve is given in Fig. 5, where the highlighted points A - D mark key stages in the beam's structural response.

The upper bound to the shear force that can be resisted at Opening 4 is given by the shear force corresponding to the pure bending resistance of the beam at the centre-line of the opening, which is a shear force of 167 kN. The increase in the load after that is due to the plasticity in the beam and to the non-linear effects of larger displacements in the FE models, which are not considered to be realistic. Therefore, the study focusses on:

- Point A (89 kN) – first yielding at the edge of the opening
- Point B (117 kN) – the start of non-linearity in the load-deflection graph
- Point C (134 kN) – full plasticity in one quadrant (the Lower Moment Side - LMS)
- Point D (165 kN) – full plasticity around the openings also with a high moment at Opening 4

Point C corresponds to a deflection of 60 mm (=span/72) and Point D to a deflection of 160 mm (=span/27), which is outside the sensible limit for use of methods that do not consider non-linear geometry of the perforated beams.

The load-deflection response was linear up to a shear load of 117 kN (Point B), as the effect of local yielding did not affect the linear load-deflection response. Von Mises contour plots (see Fig. 6a) show that the web openings experience some yielding in the four regions around the opening, starting from Opening 4 with higher global moment. The stress distribution around each opening is symmetrical with respect to the horizontal centreline of the openings in the elastic response condition, as shown in Fig. 6b.

After point B, the stresses redistribute around the openings, resulting in non-symmetrical stress patterns (Fig. 7b). The direction of the stress redistribution depends on the loading, the boundary conditions and the location of the opening on the beam. The maximum principal stresses contour plots in Fig. 7b show that the upper Tee experiences high stresses in both tension and compression, but the first fully plastic hinge (i.e. with an ultimate plastic strain ε_u = 16.5 %) eventually forms in tension on the higher moment side (HMS) at a load of 165 kN (Point D).

The FEA load-displacement curve indicates that the beam reached its full capacity at a load of 205 kN, when the plastic strains in the entire bottom Tee section exceeded the ultimate plastic strain. This high FEA shear force is not a realistic load level that can be attained without considering non-linear geometric effects. This suggests that an intermediate elasto-plastic method based on yielding around the openings before development of the full plastic resistance of the Tee sections is more likely to represent the true Vierendeel bending behaviour.

The FE analyses in the elastic range showed that stress concentrations appear at four regions in the vicinity of the web opening, which are higher on the LMS of the Tees (Fig. 6b). However, after yielding, stress redistribution from the LMS occurs towards the HMS.

There is a 41 % increase in the load capacity when the first fully plastic hinge at Point D occurs compared to the apparent limit of elastic response at Point B. At Point C (134 kN), the entire upper Tee section of Opening 4 closest to mid-span first reached its yield limit (Fig. 7a).

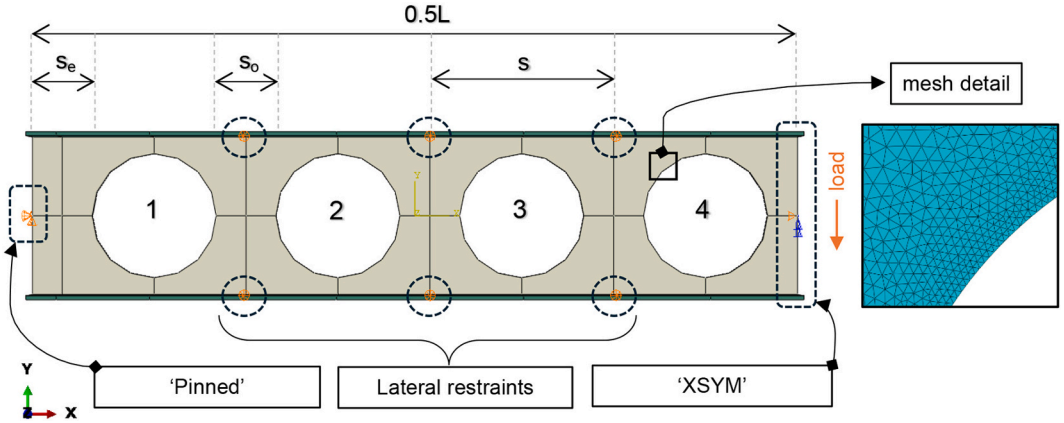

Fig. 3. Geometry nomenclature, mesh, boundary conditions and load of the four-opening beam model in Abaqus.

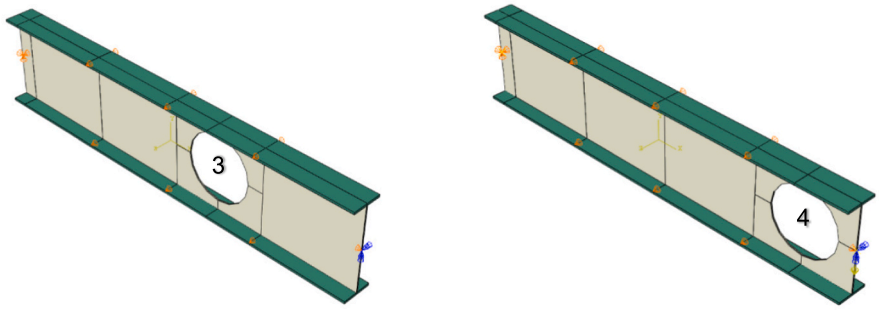

(a) *Single 3rd-opening model* ***(b)*** *Single 4th-opening model*

Fig. 4. Single-opening beams, as modelled in Abaqus. Geometry, boundary conditions and load are identical to the four-opening model, shown in Fig. 3.

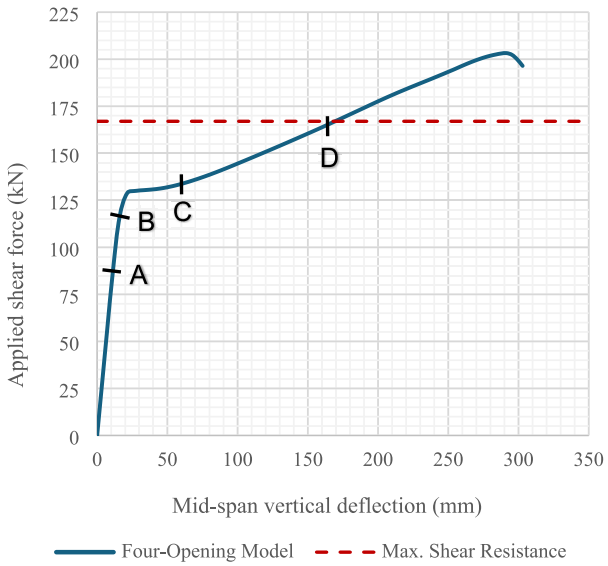

Fig. 5. Load–displacement curve for the four-opening model, as received from Abaqus using the Riks method.

The single-opening model with the opening closest to mid-span demonstrated a similar load-displacement curve, with slightly stiffer response and identical failure by *Vierendeel* bending. The rest of the single-opening models failed in tension at mid-span due to the high global bending stress, but all of them developed some level of plasticity around their openings. Hence, the single 4th-opening model is also used in the following comparisons.

3. *Vierendeel* bending design methods for circular web openings

The 'Equivalent Rectangular Opening Method' is often used for the determination of the applied moments and bending resistances of the Tee sections when designing for *Vierendeel* bending. In this method, a circular web opening is treated as an equivalent rectangular opening with an equivalent opening length and height of $0.45h_o$ and $0.9h_o$, respectively. In the reduced web section around the equivalent rectangular opening, the *Vierendeel* bending moments are calculated at the corners of the 'rectangle', which simplifies the calculations for *Vierendeel* bending design. The *Vierendeel* bending resistance of the Tees is reduced by the effect of high shear forces and high axial forces due to global bending.

The recently published Part 1–13 of Eurocode 3 [11] presents an alternative method for *Vierendeel* bending, here referred to as 'Radial Stress Method' (RSM), a linear closed-form analysis method intended to offer increased accuracy in the determination of the elastic stresses at the edge of the web opening.

3.1. Radial Stress Method (RSM)

The analysis of elastic stresses is performed by determining the equilibrium of forces and moments on radial planes around a circular web opening. A wedge is isolated from the rest of the opening by introducing a vertical plane at the centre-line of the opening and an inclined plane at angle θ from the vertical axis, as shown in Fig. 8.

The equilibrium of forces in each quadrant of the opening closest to mid-span in a region of high global moment and shear is shown in Fig. 9. Q1 is the LMS of the top T-section and Q2 is the HMS. Q4 and Q3 are the

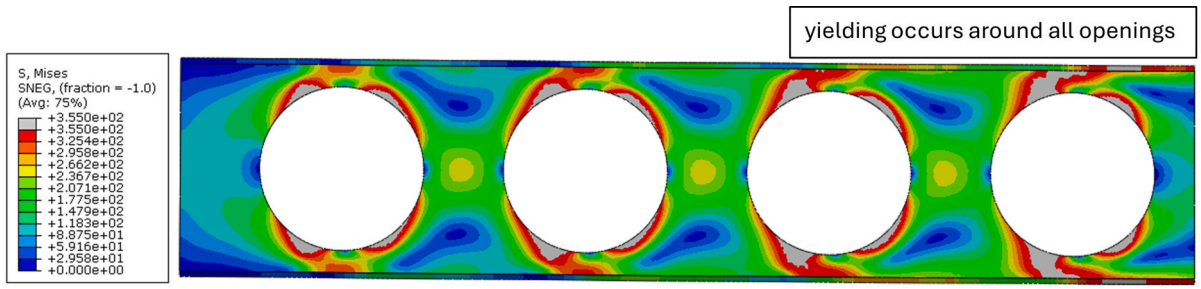

(a) *Von Mises stresses - grey contours indicate that the region has reached its yield limit.*

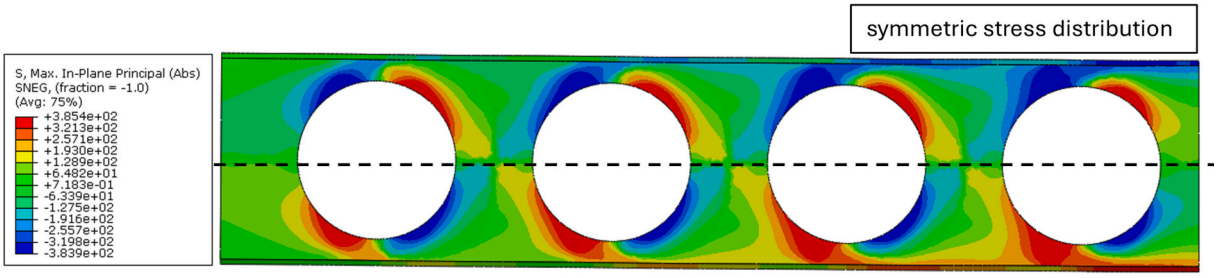

(b) *Max. at-absolute-value in-plane principal stresses.*

Fig. 6. Stress contour plots at a shear force of 117 kN - Point B in Fig. 5. The stresses are symmetric with respect to the beam's horizontal centreline while the response is elastic.

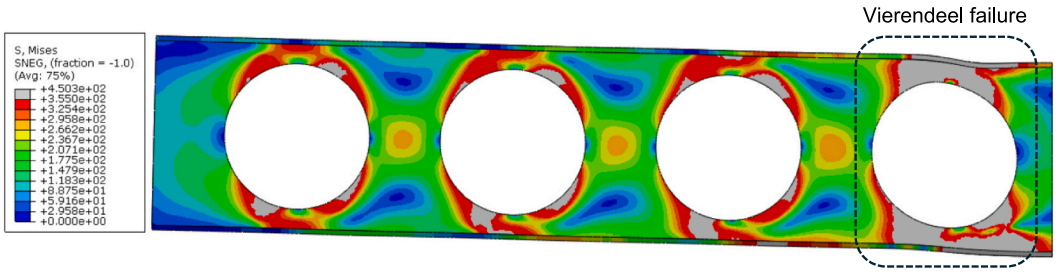

(a) *Von Mises stresses - grey contours indicate that the region has exceeded its yield limit.*

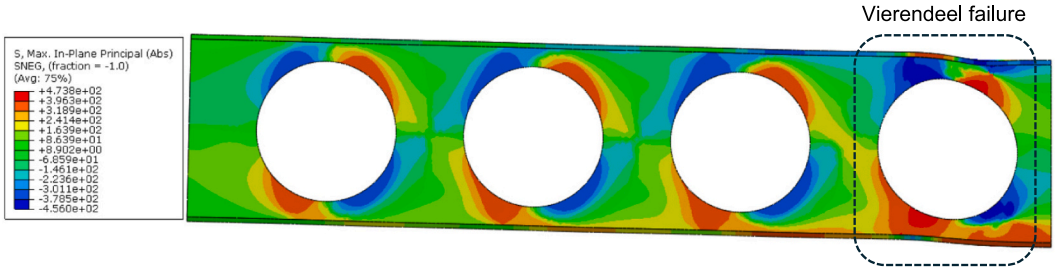

(b) *Max. at-absolute-value in-plane principal stresses.*

Fig. 7. Stress contour plots when the entire upper Tee section yields - Point C (shear force = 134 kN) in Fig. 5.

equivalent quadrants for the bottom T-section. It is apparent that the edge of the opening is in compression in the upper Tee LMS and in tension on the HMS, reversing on the bottom T-sections.

The applied shear force V_{Ed} and the normal force $N_{T,Ed}$, due to global bending, act at the centroid of the Tee section at the vertical centre-line of the opening. On a radial section at angle θ to the horizontal, the internal forces N_θ, V_θ and moment M_θ act at the elastic neutral axis of the inclined Tee cross-section. The internal normal forces and moment are calculated by considering equilibrium of forces in the isolated wedge, for increments of θ, as follows:

Q1 / LMS:

$$N_\vartheta = N_{T,Ed} \bullet \cos\vartheta + 0.5 \bullet V_{Ed} \bullet \sin\vartheta \quad (1)$$

$$V_\vartheta = N_{T,ed} \bullet \sin\vartheta - 0.5 \bullet V_{Ed} \bullet \cos\vartheta \quad (2)$$

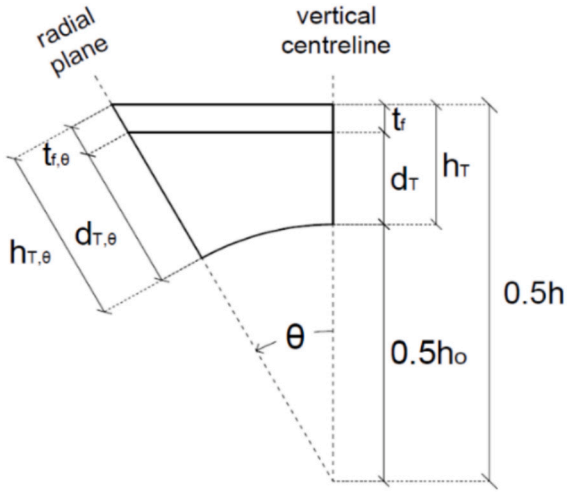

Fig. 8. 'Wedge' dimensions nomenclature, as defined by radial plane at angle θ.

$$M_\vartheta = 0.5V_{Ed} \bullet (0.5h \bullet \tan\vartheta - z_\vartheta \bullet \sin\vartheta) - N_{T,ed}(z_\vartheta \bullet \cos\vartheta - z_o) \quad (3)$$

Q2 / HMS:

$$N_\vartheta = N_{T,Ed} \bullet \cos\vartheta - 0.5 \bullet V_{Ed} \bullet \sin\vartheta \quad (4)$$

$$V_\vartheta = N_{T,ed} \bullet \sin\vartheta + 0.5 \bullet V_{Ed} \bullet \cos\vartheta \quad (5)$$

$$M_\vartheta = 0.5V_{Ed} \bullet (0.5h \bullet \tan\vartheta - z_\vartheta \bullet \sin\vartheta) + N_{T,ed}(z_\vartheta \bullet \cos\vartheta - z_o) \quad (6)$$

For Q1, the elastic normal stress in compression of the cross-section of the inclined Tee is determined at the edge of the web opening according to:

$$\sigma_{\vartheta,edge} = -\frac{N_\vartheta}{A_\vartheta} - \frac{M_\vartheta \bullet (h_{T,\vartheta} - z_\vartheta)}{I_\vartheta} \quad (7)$$

The sign convention for N_ϑ is taken as tension positive and compression negative in this formula, similarly to FEA results. For Q2, the edge stress in tension is:

$$\sigma_{\vartheta,edge} = -\frac{N_\vartheta}{A_\vartheta} + \frac{M_\vartheta \bullet (h_{T,\vartheta} - z_\vartheta)}{I_\vartheta} \quad (8)$$

Where:

- h_o is the web opening diameter;
- $h_{T,\vartheta}$ is the depth of the inclined Tee section;
- z_ϑ is the distance to the elastic neutral axis of the inclined Tee section at angle θ, measured from the top of the flange;
- z_o is the distance to the elastic neutral axis at the vertical centreline, measured from the top of the flange;
- A_θ is the area of the inclined Tee cross-section at angle θ, with $A_\vartheta = A_{f,\vartheta} + d_{T,\theta}\, t_w$;
- $A_{f,\vartheta} = b_f \bullet t_{f,\vartheta}$ is the flange area of the inclined Tee section and $t_{f,\vartheta} = t_f/cos\vartheta$;
- I_θ is the second moment of area of the inclined Tee section at angle θ.

The maximum absolute value of the normal stress on the radial plane indicates the critical cross-section in each of the four quadrants.

The modified neutral axis depth measured from the outside of the flange taking account of combined bending and compression (a negative value) is given by:

$$z_{el,\vartheta} = z_\vartheta \left(1 - \frac{N_\vartheta/A_\vartheta}{z_\vartheta \bullet M_\vartheta/I_\vartheta}\right) \quad (9)$$

$z_{el,\theta}$ is positive when it is below the top of the flange and negative when it lies above the flange. It transitions to the elasto-plastic neutral axis depth considered later.

3.2. Equilibrium interpretation of shear force in the RSM

The shear force V_ϑ on the inclined plane resulting from the equilibrium of forces in RSM does not represent the actual shear force acting in the Tee. The flange component of V_ϑ does not act as shear force in the flange but combines vectorially with the compressive axial force $N_{f,\vartheta}$ in the flange to produce the axial force along the axis of the beam. The latter is proportional to the global moment acting at the centreline of the opening, thus is of high magnitude when the global moment is high.

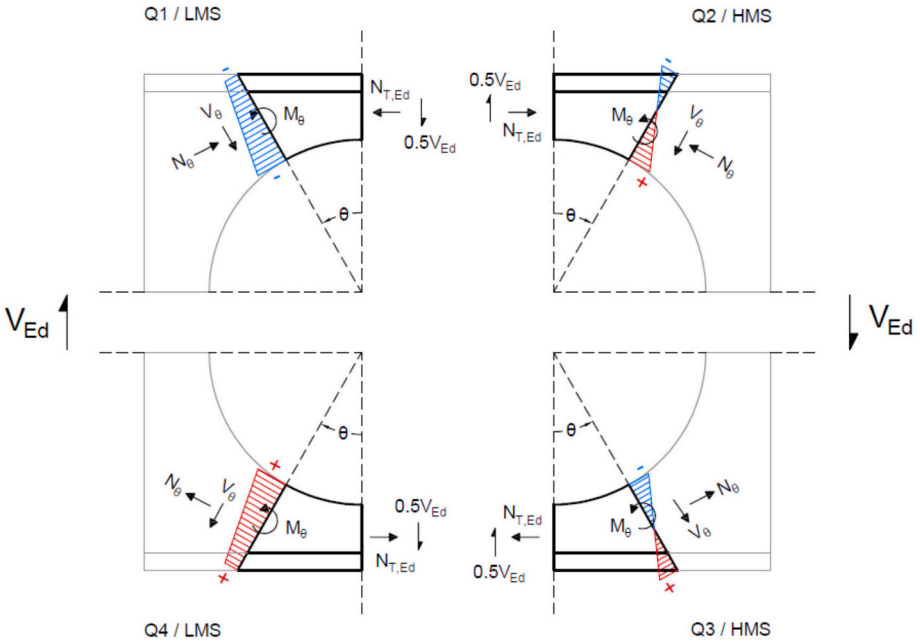

Fig. 9. Equilibrium of forces in each quadrant of the circular web opening using the RSM. The total elastic normal stress acting on the radial plane at angle θ is shown in tension (positive) and compression (negative).

The axial force acting in the flange of the inclined T-section is obtained as:

$$N_{f,\vartheta} = \left|\sigma_{\vartheta,f}\right| A_{f,\vartheta} \tag{10}$$

The combined bending and axial stress $\sigma_{\vartheta,f}$ acts at the centre of the flange, which for Q2 is given by:

$$\sigma_{\vartheta,f} = -\frac{N_\vartheta}{A_\vartheta} - \frac{M_\vartheta \bullet \left(z_\vartheta - 0.5\, t_{f,\vartheta}\right)}{I_\vartheta} \tag{11}$$

The inclined shear force acting the flange may be calculated from the axial force $N_{f,\vartheta}$ as:

$$V_{f,\vartheta} = N_{f,\vartheta} \tan\vartheta \tag{12}$$

Finally, the actual shear force $V_{w,\vartheta}$ acting in the web of the inclined Tee section (Fig. 10) is given by:

$$V_{w,\vartheta} = V_\vartheta - V_{f,\vartheta} \tag{13}$$

For this shear force, the transverse shear stress acting on the inclined T-section follows a parabolic distribution, with a maximum value at the neutral axis. The shear stress is given by:

$$\tau_\theta = \frac{V_{w,\theta} \bullet Q_\theta}{I_\vartheta \bullet t_w} \tag{14}$$

Where:

- Q_θ is the first moment of area about the neutral axis, at a particular web section of the inclined cross-section at angle θ;
- t_w is the thickness of the web.

The shear stress in the elastic portion of the inclined Tee section increases when plasticity of the inclined web increases, but generally the shear stresses only have an effect when the web is close to being fully plastic.

3.3. Comparison between RSM and FEA results

The ability of the RSM to reliably estimate the normal stresses at the edge of the web opening is investigated in this section. These normal stress estimations are compared to the FEA results using geometrically and materially non-linear properties. The analytical method leads to elastic stresses and therefore the comparison with the non-linear FEA is only relevant up to the elastic limit at the edge of the most highly stressed sector of the opening (Point B in Fig. 5).

The RSM is used to calculate the stresses at incremental angles (maximum of 5°) around the openings in order to determine the maximum edge stress in each of the four quadrants. For low global moments, the critical planes are at 20 to 25° the vertical centre-line, but as the primary moment increases, the angle of the critical planes reduces for the LMS and increases for the HMS. The RSM critical angles generally agree well with the FEA analyses.

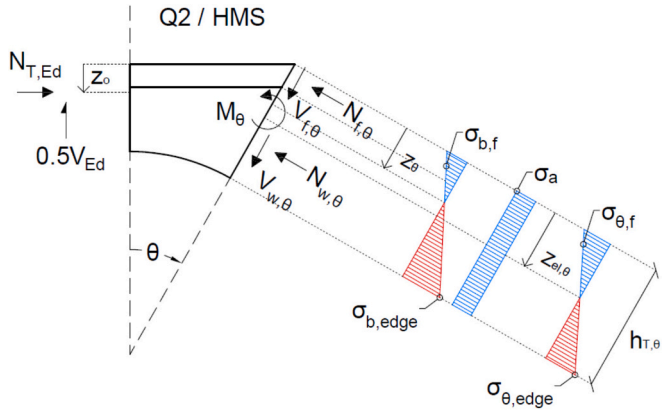

Fig. 10. Force equilibrium in the RSM, shown for the HMS in Q2.

The use of the RSM to determine the critical radial plane is presented in Table 3 for each of the web openings of the four-opening model as shown in Fig. 3. The comparison is made at the load corresponding to the edge stress equal to f_y in the FEA (Fig. 6a). It is seen that the maximum shear force is 108 kN at Opening 4 and 95 kN at Opening 1, in both cases at the HMS (Q2).

Regarding the RSM's results, the elastic normal stresses are calculated separately for each quadrant around the web opening, on one-degree increments of θ. The latter is measured from the vertical centreline to the horizontal centreline, as shown in Fig. 9. For presentation purposes, the normal stress results are presented in terms of a continuous angle φ, where φ is measured clockwise from the horizontal centreline of the openings (starting with Q1 in Fig. 11).

The difference between shear forces corresponding to yielding at the LMS (Q1) and the HMS (Q2) of the opening increases as the effect of global moment increases. For Opening 1, the difference in the peak stresses between the two sides of the opening is small (7 %), but increases to 33 % at Opening 4 because of the effect of the high global moment (of 214 kNm). The critical angle to the vertical, which represents the position of highest edge stress also increases by 5° on the HMS and reduces by 4° on the LMS.

The maximum absolute in-plane principal stress components were extracted from Abaqus to be used in a more detailed comparison. This principal stress component is useful in this study because its vector at the edge of the web opening is tangential to the edge of the circular web opening, similarly to the RSM's normal stress $\sigma_{\vartheta,edge}$. In this context, it is sensible to set the FEA principal stress results as benchmark to assess the accuracy of the RSM.

Three different stress states of the web opening close to mid-span are identified in the linear response of the FE model, with the first stress state corresponding to a shear force of 54 kN. The second stress state was identified at 89 kN (Point A – Fig. 5) where some shear-moment interaction occurs because the shear force on the radial plane exceeded half of the plastic shear resistance ($V_\vartheta > 0.5V_{\vartheta,pl,Rd}$) in accordance with [22]. Finally, the third stress state was identified as the Point B at a shear force of 117 kN where the FE response is no longer elastic due to local yielding at the edge of the openings.

The analytical RSM and the non-linear FEA stress results for the three loads are presented in Fig. 12 in which the normal stress at the edge of the opening is shown as a function of the radial angle φ (measured from the horizontal axis of the beam). The edge stress on the vertical axis corresponds to the elastic normal stress at the edge of the opening for the RSM and to the maximum at-absolute-value in-plane principal stress for

Table 3
Maximum shear forces at the four openings corresponding to first yielding at the edge of the opening at the critical angle to the vertical.

Opening	Ratio: M_{Ed}/V_{Ed}	Sector	Shear force V_{Ed} at elastic limit	Critical angle θ_{cr} to the vertical
1	0.33	Q1 (LMS)	88 kN	22°
		Q2 (HMS)	95 kN	24°
2	0.83	Q1 (LMS)	83 kN	20°
		Q2 (HMS)	100 kN	26°
3	1.33	Q1 (LMS)	78 kN	19°
		Q2 (HMS)	104 kN	27°
4	1.83	Q1 (LMS)	73 kN	18°
		Q2 (HMS)	108 kN	29°

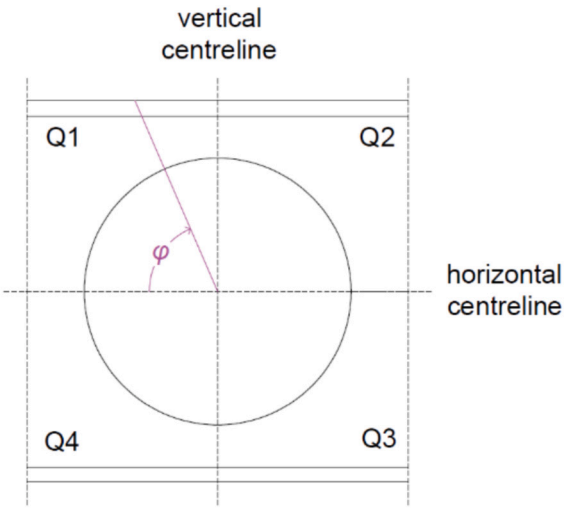

Fig. 11. Radial angle φ relative to the longitudinal axis of the beam used to present the radial stresses around a circular opening.

the FEA results, respectively.

The differences in the FEA results between the four-opening model and the single-opening model are negligible except in quadrants Q1 and Q4, of the 4-opening model at the radial planes within 45° from the horizontal centreline, due to the interaction between the openings closest to mid-span. Conversely, the stresses acting on the radial planes within 45° from the vertical centreline correspond to *Vierendeel* bending, which is the scope of this paper. Hence, the single-opening model is used as a reference to both FEA results in the following comparison.

At a shear force of 54 kN (Fig. 12a), the RSM determines the maximum stresses at the edge of the web opening with reasonable accuracy. Both the analytical and the FEA results produce a characteristic 'S' stress distribution, also reported in [9], with maximum (absolute) value stresses in Q1 and Q4. In all quadrants, the RSM's stress estimations are up to 21 % lower in magnitude than given by the FEA. In Q1 and Q4, the RSM and FEA agree well on the angle of the critical plane, while in Q2 and Q3 a difference of approximately 10° is observed.

At the shear force of 89 kN (Fig. 12b), a plateau is observed in the stresses on the critical radial planes of the FEA results, which are more prominent in Q1 and Q4 and represent the extent of localised yielding at the edge of the openings. The RSM elastic stresses are proportional to the applied load and the peak stresses are up to 22 % higher than in FEA in Q1 and Q4, and up to 18 % lower in Q2 and Q3.

At Point B for a shear force of 117 kN (Fig. 12c), the plateaux are even more pronounced, indicating that large part of the edge of the opening has reached its yield limit.

These limits of the RSM can be attributed to two reasons; Firstly, it is an elastic method that does not take into consideration the development of plastic stresses, which lead to significant stress redistribution. Secondly, the method ignores the possible effect of shear-moment interaction on the radial plane, which although small, may affect the local yielding as observed in the FEA.

In this paper, the elastic method is extended to consider the elasto-plastic behaviour of the Tee sections and the redistribution of moments between the two sides of the opening as the plasticity develops.

3.4. Comparison between FEA and the Equivalent Rectangular Opening Method

The Equivalent Rectangular Opening Method is presented in detail in the Appendix. It is shown that the maximum shear force due to the Vierendeel bending resistance in the absence of high shear and global moment is 199 kN based on the plastic bending resistance of the Tees. This reduces to 175 kN for Opening 1 considering the effect of the shear force on the local bending resistances of the Tees and then to 111 kN for Opening 4 considering the effect of the high axial forces at the opening closest to mid-span.

From the FEA, the comparable shear force is 134 kN, which corresponds to the yielding of the entire upper Tee section (Fig. 7a). The corresponding shear force due to the elastic bending resistance of the Tees is 103 kN. This may be compared to the proportionate limit of 117 kN obtained from the FEA. It follows that the equivalent rectangle method is relatively conservative for Opening 4 based on the FEA results.

4. *Enhanced RSM* to account for plasticity in the Tee section

After first yielding has occurred at the edge of the opening, yielding of the inclined web then extends towards the flanges, resulting in an increase in the bending resistance of the inclined Tee section. In the following elasto-plastic theory, the development of the plasticity in the Tees may be followed incrementally with the applied load, which is limited either by development of the full plastic bending resistance of the Tee section or by local buckling depending on the slenderness of the web.

4.1. RSM-based elasto-plastic stress analysis on the inclined Tee section

The elasto-plastic stress regime is shown in Fig. 13 in which the radial strain at the edge of the opening is $n{\cdot}\varepsilon_y$, where $\varepsilon_y = f_y / E$. Therefore, as the value on 'n' increases, so does the depth of the plastic stress block in the web. The elasto-plastic neutral axis depth from the outside of the flange gradually reduces as the strain in the flange of the inclined T-section increases.

The force equilibrium in Q1 is given by Eq. (1) and Eq. (2), while in Q2 by Eq. (4) and Eq. (5). The applied moment M_θ, acting on the inclined Tee section about the elasto-plastic neutral axis, $z_{ep,\theta}$ is given for Q1 by:

$$M_\vartheta = 0.5V_{Ed} \bullet \left(0.5h \bullet \tan\vartheta - z_{ep,\vartheta} \bullet \sin\vartheta\right) - N_{T,ed}\left(z_{ep,\vartheta} \bullet \cos\vartheta - z_o\right) \quad (15)$$

In this equation, $z_{ep,\theta}$ is negative when it lies outside the flange and positive when it lies inside the inclined T-section.

The corresponding equation for the applied moment in Q2, where $z_{ep,\theta}$ is positive, is given by:

$$M_\vartheta = 0.5V_{Ed} \bullet \left(0.5h \bullet \tan\vartheta - z_{ep,\vartheta} \bullet \sin\vartheta\right) + N_{T,Ed}\left(z_{ep,\vartheta} \bullet \cos\vartheta - z_o\right) \quad (16)$$

The elasto-plastic neutral axis, as well as the stresses and strains in the inclined Tee section can be determined as a function of the post-elastic strain $n{\cdot}\varepsilon_y$ and the yield stress f_y at the edge of the opening. A process of iteration is required to determine the value of n and the elasto-plastic neutral axis position $z_{ep,\vartheta}$ with respect to the applied moment and forces.

4.1.1. Case 1: Neutral axis within the Tee section

In Q2, the elasto-plastic neutral axis depth, $z_{ep,\theta}$ generally lies in the web of the inclined T-section, as shown in Fig. 14.

Equilibrium of in-plane forces for an applied axial force, N_ϑ, when based on post-elastic strains in the web of the Tee section, is given by:

$$N_\vartheta = nA_f\left(\frac{z_{ep,\vartheta} - 0.5\,t_{f,\vartheta}}{h_{T,\vartheta} - z_{ep,\vartheta}}\right)f_y + n\,t_w\frac{\left(z_{ep,\vartheta} - t_{f,\vartheta}\right)^2}{2\left(h_{T,\vartheta} - z_{ep,\vartheta}\right)}f_y - t_w\left(\frac{2n-1}{2n}\right)\left(h_{T,\vartheta} - z_{ep,\vartheta}\right)f_y \quad (17)$$

Expanding Eq. (17) and rewriting in terms of the variable $z_{ep,\vartheta}$ as a function of 'n' results in the following quadratic equation:

$$A \bullet {z_{ep,\vartheta}}^2 + B \bullet z_{ep,\vartheta} + C = 0 \quad (18)$$

The solution for $z_{ep,\vartheta}$ is obtained from:

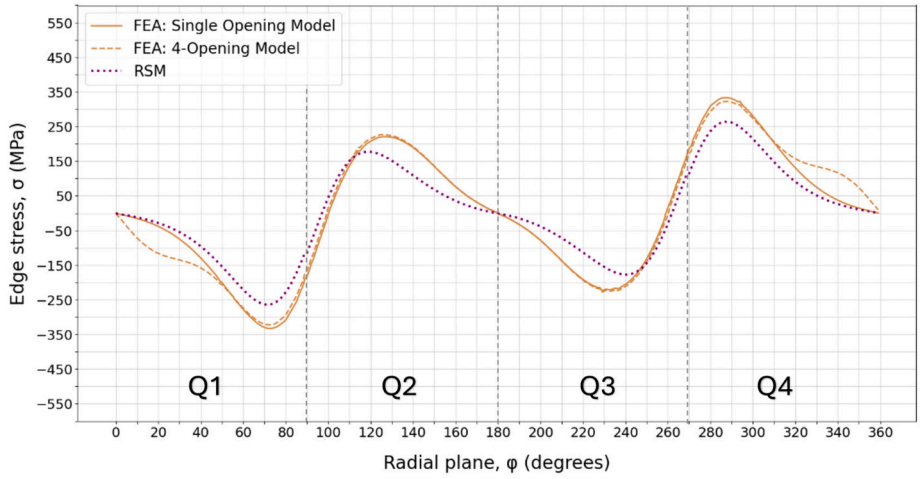

(a) *Stress state 1 at a load of 54 kN (elastic behaviour)*

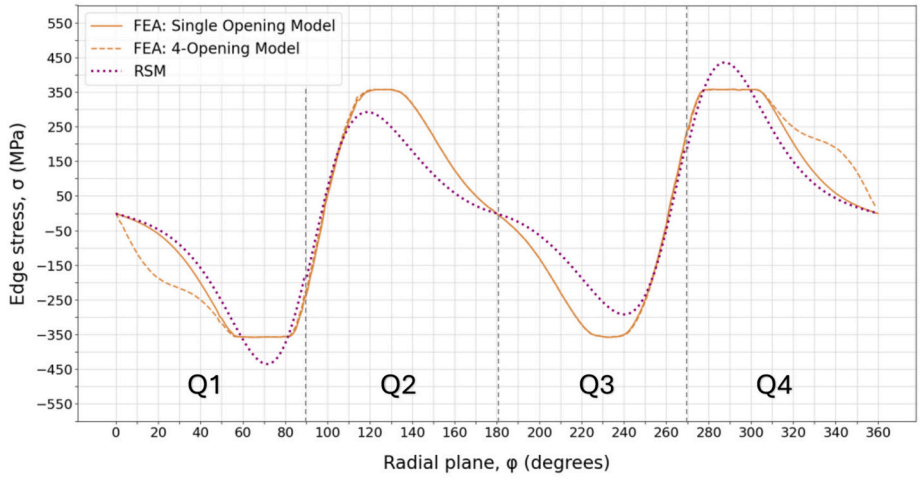

(b) *Stress state 2 at a load of 89 kN (Point A – Fig. 5)*

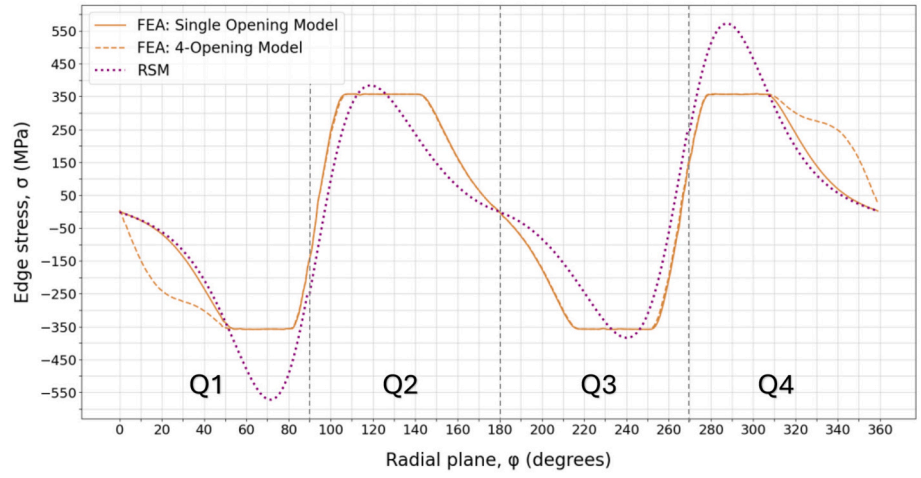

(c) *Stress state 3 at a load of 117 kN (Point B – Fig. 5)*

Fig. 12. Radial stress distribution at the edge of the opening closest to mid-span as a function of the angle φ relative to the longitudinal axis of the beam.

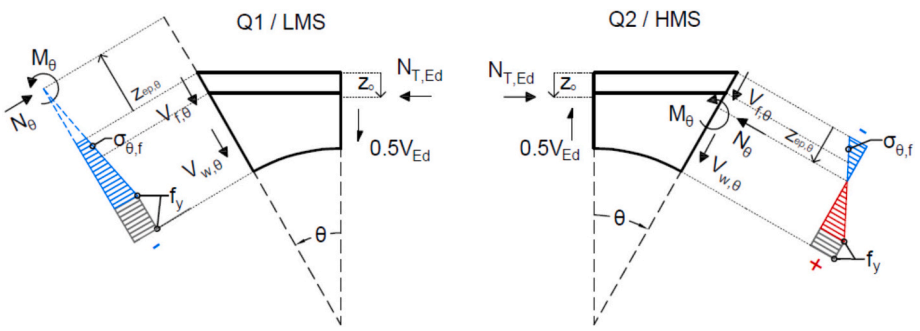

Fig. 13. Enhanced RSM equilibrium of forces in the upper Tee. The value of $z_{ep,\vartheta}$ is negative when the elasto-plastic neutral axis lies above the T-section, as in Q1.

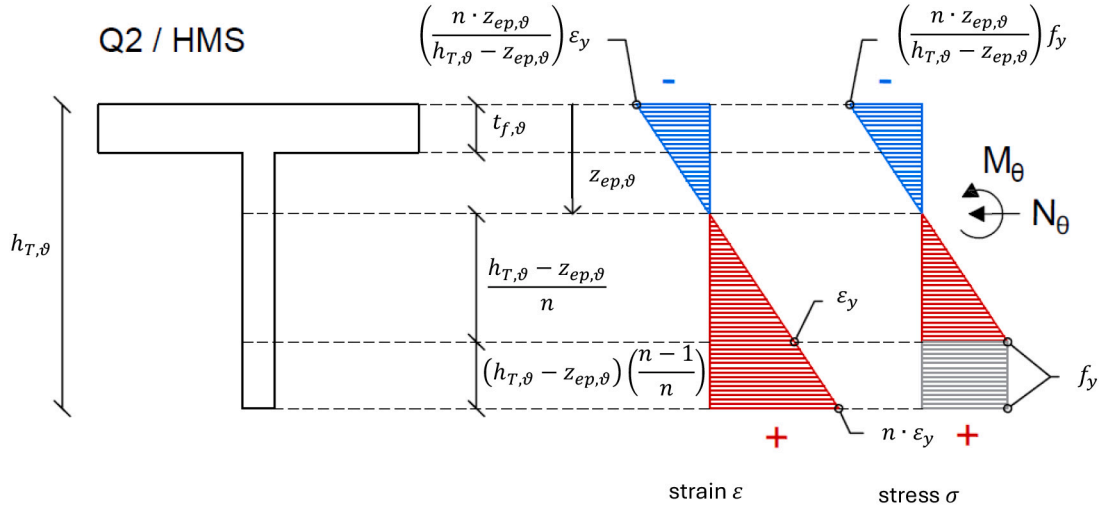

Fig. 14. Elasto-plastic stress and strain distribution as a function of $n \cdot \varepsilon_y$ in the inclined Tee section of Q2. The value of $z_{ep,\vartheta}$ is positive in Q2.

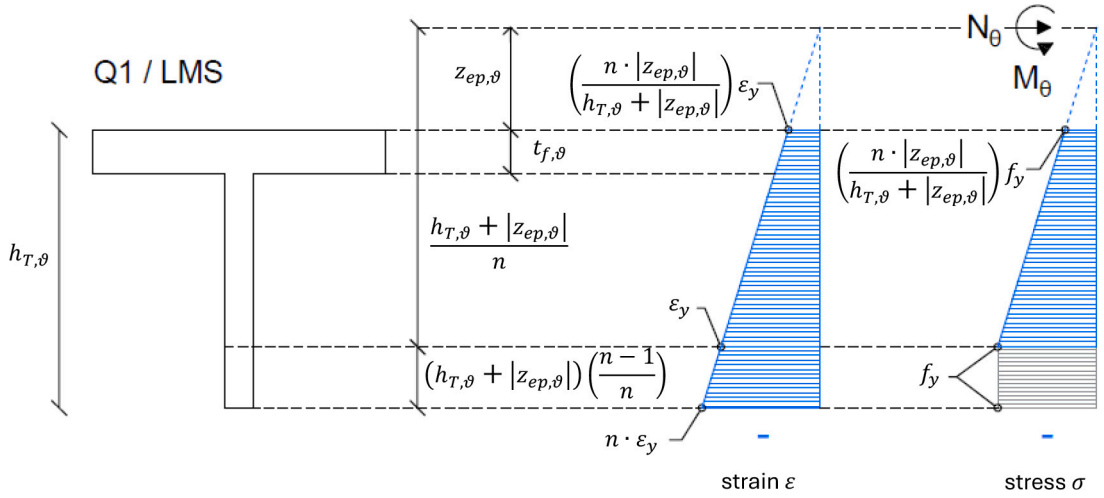

Fig. 15. Elasto-plastic stress and strain distribution as a function of $n \cdot \varepsilon_y$ in the inclined Tee section of Q1. The value of $z_{ep,\vartheta}$ is negative in Q1.

$$z_{ep,\vartheta} = \frac{-B \pm \sqrt{B^2 - 4\,A\,C}}{2A} \tag{19}$$

where:

$$A = \left[\frac{(n-1)^2}{2n} t_w\right] \tag{20}$$

$$B = \left[n\,A_{f,\vartheta} + \frac{N_\vartheta}{f_y} + t_w\left(\frac{2n-1}{n} h_{T,\vartheta} - n\,t_{f,\vartheta}\right)\right] \tag{21}$$

$$C = -\left[0.5\,n\,t_{f,\vartheta}\,A_{f,\vartheta} + \frac{N_\vartheta}{f_y}\,h_{T,\vartheta} + 0.5 t_w\left(\frac{2n-1}{n} {h_{T,\vartheta}}^2 - n\,{t_{f,\vartheta}}^2\right)\right] \tag{22}$$

As a good approximation for smaller values of 'n', $z_{ep,\vartheta} = -C/B$, which also applies for the elastic limit ($n = 1$).

4.1.2. Case 2: Neutral axis outside the Tee section

In the case of Q1, the entire Tee section acts in compression. The elasto-plastic neutral axis now lies above the Tee as shown in Fig. 15, and so is a negative value.

Equilibrium of in-plane forces for an applied axial force, N_ϑ, and rewriting in terms of the $z_{ep,\vartheta}$ leads to a quadratic equation in the form of Eq. (18), with the same term A as given for Q2, but the terms B and C are now:

$$B = \left[n\,A_{f,\vartheta} - \frac{N_\vartheta}{f_y} + t_w\left(\frac{2n-1}{n} h_{T,\vartheta} - n\,t_{f,\vartheta}\right)\right] \tag{23}$$

$$C = -\left[0.5\,n\,t_{f,\vartheta}\,A_{f,\vartheta} - \frac{N_\vartheta}{f_y}\,h_{T,\vartheta} + 0.5 t_w\left(\frac{2n-1}{n} {h_{T,\vartheta}}^2 - n\,{t_{f,\vartheta}}^2\right)\right] \tag{24}$$

4.2. Elasto-plastic bending resistance of the Tee section

For a given axial force N_θ and moment M_θ on the inclined T-section, the elasto-plastic bending resistance of the inclined T-section can be determined by taking moments about the neutral axis position, $z_{ep,\vartheta}$. For Case 1 (Q2), the elasto-plastic bending resistance of the T-section for N + M interaction is given by:

$$M_{Rd,ep,\vartheta} = n\,A_{f,\vartheta}\frac{(z_{ep,\vartheta} - 0.5t_{f,\vartheta})^2}{h_{T,\vartheta} - z_{ep,\vartheta}} f_y + n\,\frac{(z_{ep,\vartheta} - t_{f,\vartheta})^3}{3(h_{T,\vartheta} - z_{ep,\vartheta})} t_w f_y + \frac{(3n^2-1)}{6n^2}(h_{T,\vartheta} - z_{ep,\vartheta})^2 t_w f_y \tag{25}$$

The level of plasticity that the web of the inclined Tee section can develop, expressed through the value of n, can be determined by solving iteratively in terms of n until $r = 1$, where r is the ratio $M_\vartheta / M_{Rd,ep,\vartheta}$.

A small additional term is due to the bending resistance of the flange because of the strain across it. This term is given below, and is more important for Tee sections with thicker flanges:

$$M_{Rd,fl,\vartheta} = \frac{n\,A_{f,\vartheta}\,{t_{f,\vartheta}}^2}{12\,(h_{T,\vartheta} - z_{ep,\vartheta})} f_y \tag{26}$$

The total elasto-plastic bending resistance of the Tee section is calculated as:

Table 4
Enhanced RSM results for Opening 4 (for Q2, θ = 25°), at a shear force of 117 kN.

n	$z_{ep,\vartheta}$ (mm)	$M_{Rd,ep,\vartheta}$ (kNm)	$M_{Rd,fl,\vartheta}$ (kNm)	$M_{Rd,tot,\vartheta}$, (kNm)	M_ϑ (kNm)	r	Yielded web depth (%)
1.05	35.93	16.12	0.19	16.31	16.34	1.002	3.1
1.06	35.79	16.10	0.19	16.29	16.28	0.999	3.7
1.10	35.25	16.03	0.20	16.23	16.05	0.989	6.0

Table 5
Enhanced RSM results for Opening 4 (for Q1, θ = 25°), at a shear force of 117 kN.

n	$z_{ep,\vartheta}$ (mm)	$M_{Rd,ep,\vartheta}$ (kNm)	$M_{Rd,fl,\vartheta}$ (kNm)	$M_{Rd,tot,\vartheta}$, (kNm)	M_ϑ (kNm)	r	Yielded web depth (%)
7.15	1.06	9.59	0.71	10.30	10.74	1.043	99.9
11.30	2.95	8.69	1.16	9.84	9.85	1.001	103.4
11.35	2.96	8.68	1.16	9.84	9.84	1.000	103.5

$$M_{Rd,tot,\vartheta} = M_{Rd,ep,\vartheta} + M_{Rd,fl,\vartheta} \tag{27}$$

For Case 2 (Q1) where the entire cross-section is under compression, the elasto-plastic neutral axis lies above the flange and $z_{ep,\vartheta}$ is negative in Eq. (25) and Eq. (26).

First, the Enhanced RSM is examined at a shear force of 117 kN (Point B in Fig. 5) where some plasticity in the edge of the web has occurred around the opening closest to mid-span (Opening 4) but the overall beam response is linear elastic from the load-displacement graph. The results at θ = 25° are presented in Tables 4 and 5 for Q2 and Q1 respectively. For Q2, the calculated value of $n = 1.06$ indicates a small degree of plasticity in this sector, while for Q1 the substantially higher level of plasticity occurs with a calculated value of $n = 11.35$. However, at θ = 25° the value of $n = 7.15$ represents the maximum attainable plasticity level in the web, thus values of n above that should be ignored. The latter agrees well with the FEA results (Fig. 6a), where the grey contours show clearly that larger part of the Tee's web has yielded on the LMS. This suggests that some redistribution of moment occurs from Q1 to Q2 in order to satisfy equilibrium at Opening 4, which is investigated later.

Next, the method was examined at a lower shear force of 89 kN (Point A in Fig. 5) for both sectors. For Q2 no yielding was observed, while for Q1 the values for $n = 1.20$ showed that about a quarter of its web depth yielded (Table 6).

Finally, at a higher shear force of 134 kN (Point C in Fig. 5) the method resulted in the increased plasticity of $n = 1.25$ for Q2 (Table 7), but in Q1 the entire web outstand had already developed its full plastic capacity at a lower shear force of 117 kN. This is in general agreement with the non-linear FEA results in Fig. 7a; but the FEA contour plots suggest a more balanced stress distribution between the HMS and the LMS.

This shows that redistribution of moment between Q1 and Q2 and between Q4 and Q3 is required in order to develop the plastic bending resistances of the four sectors (Q1 to Q4) around Opening 4 in particular, which leads to the proposed adaptation of the RSM - see Section 4.4.

The use of the Enhanced RSM in Q3 and Q4 is similar to Q2 and Q1 respectively, but the axial stress is in tension in the bottom Tee.

4.3. Sensitivity of the Enhanced RSM to global moment

A sensitivity analysis study was conducted to further evaluate the performance of the Enhanced RSM. All openings of the four-opening model developed plasticity around them (Fig. 6a), and are examined in this section in an effort to assess the effect of the global bending moment on the elasto-plastic stress analysis on the inclined Tee section, as well as the Enhanced RSM capacity to identify the level of plasticity in each sector. The results for the shear force at Openings 1 to 4 corresponding to different values of 'n' at sectors Q1 and Q2 are presented in Table 8. It should be noted that the Enhanced RSM treats each opening as an isolated opening given a shear-moment ratio acting at the opening's centreline.

The change in the critical angle θ_{cr} between the elastic limit and the elasto-plastic response for $n = 2$ is shown by comparing Tables 8 and 3, with the critical angle at the elastic limit also being the critical angle throughout the elasto-plastic response.

Full plasticity of the inclined Tee section may be taken to occur for n

Table 6
Enhanced RSM results for Opening 4 (for Q1, θ = 25°), at a shear force of 89 kN.

n	$z_{ep,\vartheta}$ (mm)	$M_{Rd,ep,\vartheta}$ (kNm)	$M_{Rd,fl,\vartheta}$ (kNm)	$M_{Rd,tot,\vartheta,}$ (kNm)	M_{ϑ} (kNm)	r	Yielded web depth (%)
1.15	−25.14	17.48	0.09	17.56	17.66	1.005	20.2
1.20	−22.82	16.75	0.09	16.84	16.82	0.999	25.3
1.25	−20.83	16.12	0.10	16.22	16.10	0.992	29.7

Note: The value of $z_{ep,\vartheta}$ is negative, indicating that the elasto-plastic neutral axis is above the Tee as shown in Fig. 15.

Table 7
Enhanced RSM results for Opening 4 (for Q2, θ = 25°), at a shear force of 134 kN.

n	$z_{ep,\vartheta}$ (mm)	$M_{Rd,ep,\vartheta}$ (kNm)	$M_{Rd,fl,\vartheta}$ (kNm)	$M_{Rd,tot,\vartheta,}$ (kNm)	M_{ϑ} (kNm)	r	Yielded web depth (%)
1.20	35.90	18.32	0.22	18.53	18.70	1.009	10.8
1.25	35.30	18.18	0.22	18.40	18.40	1.000	13.1
1.30	34.71	18.04	0.23	18.27	18.12	0.992	15.3

Table 8
Shear forces and critical angles θ_{cr} corresponding to increasing levels of elasto-plastic behaviour for Q1 and Q2 of the four openings.

Opening	Ratio: M_{Ed}/V_{Ed}	Sector	n = 1.5	n = 2	n = 3	n = 4	n = 5
1	0.33	Q1 (LMS)	112 kN (22°)	122 kN (22°)	130 kN (22°)	135 kN (23°)	138 kN (23°)
		Q2 (HMS)	123 kN (24°)	136 kN (24°)	149 kN (24°)	155 kN (25°)	160 kN (25°)
2	0.83	Q1 (LMS)	104 kN (20°)	111 kN (20°)	117 kN (20°)	121 kN (21°)	124 kN (21°)
		Q2 (HMS)	131 kN (25°)	147 kN (25°)	163 kN (26°)	172 kN (26°)	178 kN (26°)
3	1.33	Q1 (LMS)	95 kN (18°)	101 kN (18°)	105 kN (19°)	108 kN (19°)	111 kN (19°)
		Q2 (HMS)	137 kN (28°)	156 kN (28°)	177 kN (28°)	189 kN (29°)	196 kN (29°)
4	1.83	Q1 (LMS)	90 kN (14°)	91 kN (15°)	95 kN (17°)	97 kN (17°)	100 kN (18°)
		Q2 (HMS)	143 kN (29°)	164 kN (29°)	*190 kN (30°)	*205 kN (30°)	*215 kN (30°)

Note: The shear forces V_{Ed} denoted with an asterisk (*) exceed the upper bound of 167kN, which depends on the bending resistance of the cross-section at the centre-line of Opening 4. Hence, the respective levels of plasticity 'n' are not attainable.

= 5, at which point most of the web has yielded. It is seen that for all shear-moment ratios the maximum shear force is lower in Q1 than in Q2, indicating that the LMS is critical.

Table 8 also shows that for low shear-moment ratios the critical planes for Q1 and Q2 are found at angles that are near-symmetrical to the vertical, between 20° and 25°, while for higher ratios the critical angles are more skewed towards the HMS. Additionally, it is seen that the difference in the critical shear forces between Q1 and Q2 is greater for the higher shear-moment ratios, which suggests that only low plasticity levels may be attained in HMS for Openings 3 and 4.

Fig. 16 shows the depth of the yielded web in the upper Tee sectors Q1 and Q2 around Openings 1 to 4 for a shear force of 117 kN. The figure also illustrates how the critical angle θ_{cr} changes for different ratios of global moment and shear force.

In Q2, more plasticity is observed in the inclined web for the cases of lower global moment, M_{Ed}. Conversely, in Q1, a higher global moment M_{Ed} results in higher level of plasticity in the web. More specifically, in Q1 the entire web outstand has yielded in the range of 15° to 23° and 10° to 27° for global moments of 156 kNm and 214 kNm in Openings 3 and 4 respectively.

Both plots show that the global moment to shear force ratio has an effect on the critical angle θ_{cr}, which is represented by the angle θ where the yielded web depth ratio is greatest. In both sectors, the higher levels of plasticity are observed at angles closer to the vertical centre-line. There is also a slight difference between the critical angle position in the elastic and elasto-plastic conditions.

4.4. Moment redistribution in the Tee

It is clear from the FEA results that redistribution of moments occurs from Q1 to Q2, and from Q4 to Q3, in order to allow both sides to develop their plastic capacity. At the most highly stressed Opening 4, the moment in Q1 is reduced and increased in Q2. This may be represented by a small movement in the position of zero bending from the centre-line of the opening towards Q1, as shown in Fig. 17. This change in moment acting on the inclined Tee sections is given by:

$$\Delta M_T = 0.5\, V_{Ed}\, e \tag{28}$$

where e is the movement in the position of zero bending from the centre-line of the opening.

The shear force corresponding to various 'n' values in both sectors is taken as the failure load allowing for a small redistribution of moment. These results are presented in Table 9.

The maximum value of ΔM_T is also given by the bending resistance of the Tee section at the centre-line of the opening in combination with the axial force due to global bending. For Opening 4 subject to high global moment, the bending resistance of the Tee section is calculated as 2.4 kNm for a shear force of 117 kN and 1.7 kNm for a shear force of 134 kN. This corresponds to maximum values of e ≤ 41 mm for V = 117 kN and e ≤ 25 mm for V = 134 kN.

Table 9 presents the value of 'n' for Opening 4 at a shear force of 117 kN, for the cases of θ = 15° and θ = 25°. For θ = 25°, a moment redistribution of ΔM_T = 1.35 kNm, determined in Q1 at n = 1.5 for which r' ≈ 1 in Q2, results in equilibrium in both sides of the opening. This redistribution corresponds to a movement of e = 23.2 mm in the line of zero moment. Slightly higher moment redistribution is calculated for θ = 15° and plasticity level n ≈ 1.25. This analysis was repeated for a shear force of 134 kN (Point C in Fig. 5). For θ = 25°, the plasticity limit is found at n ≈ 2.5 which allows for a redistribution of ΔM_T = 2.21 kNm, but this moment exceeds the bending resistance of the T-section at the centre-line of the opening.

It was found from this study that the maximum shear force for Opening 4 is calculated to be 127 kN, when limited by the redistribution of moment between Q2 and Q1. This is clearly less than the shear force predicted by the FEA which includes geometric and material non-linearity. However, the shear force is 74 % higher than the shear force for elastic design of Q1 (LMS) at Opening 4.

A further constraint on the shear resistance of slender webs may be

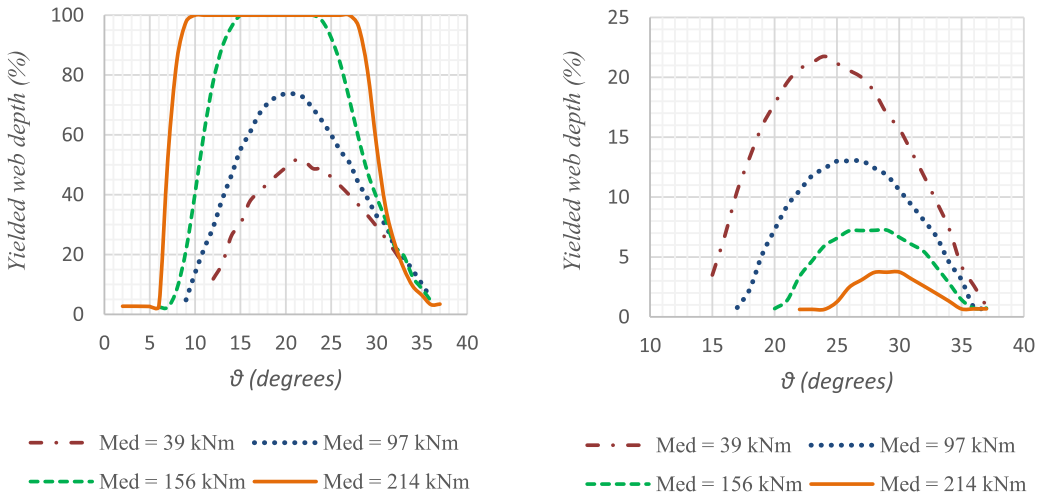

Fig. 16. Level of plasticity in the inclined web outstands for each of the four openings at a shear force of 117 kN.

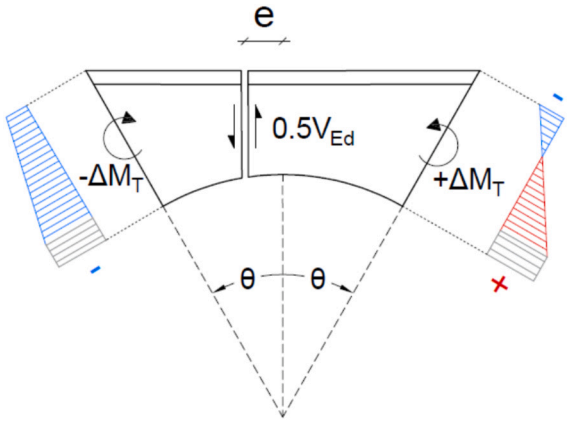

Fig. 17. Redistribution of moment from Q1 to Q2 due to movement in point of zero moment at Opening 4.

buckling of the web if the edge stress next to the opening reaches the critical buckling stress in Q1 and Q3. However, the web is tension in Q2 and Q4 is able to resist a higher shear force. In this case, it may be required to limit the compression stress at the edge of the opening in Q1 although the tension stress in Q2 can reach yield and can develop its elasto-plastic bending resistance by a redistribution of moment, ΔM_T to Q2. The FEA results in this case show that local buckling around the opening did not occur for $h_o \leq 55t_w\varepsilon$.

4.5. Experimental validation of the Enhanced RSM

This section presents a validation of the proposed analytical method against experimental data from the literature. Four tests on simply supported cellular beams failing in Vierendeel bending are utilised for this purpose. Three tests (specimens W-1A, W-2A, and W-3A) use data from [23], while a fourth test case (T-1) is from [15,16]. The key geometric and material properties of the selected specimens are given in Table 10.

The comparison between the failure loads captured during the tests and the Enhanced RSM predictions is presented in Table 11. It is shown that the proposed method demonstrates excellent agreement with the experimental results (on average: $V_{E.RSM}/V_{exp} = 0.84$ and $V_{E.RSM}/V_{exp} = 0.94$ with moment redistribution), and provides higher accuracy than the Equivalent Rectangular Opening Method (on average: $V_{EqR}/V_{exp} = 0.77$). For two of the Warren tests, the Enhanced RSM method over-predicts the failure load by 2 and 3 % but this may be due to some local buckling around the slender webs in the test cases. For specimen T-1, the end-post with its end plate adjacent to the web opening likely contributed to its higher test failure load compared to the Enhanced RSM prediction.

This shows that the Enhanced RSM method gives good predictions of the Vierendeel bending resistance around circular openings allowing for redistribution of moments.

Table 9
Redistribution of moment at Opening 4 for $V_{Ed} = 117$ kN ($M_{Ed}/V_{Ed} = 1.83$).

		No redistribution of moment						With redistribution of moment				
		Q1 (LMS)			Q2 (HMS)			Q1 → Q2		Q1	Q2	
	n	$M_{\theta,Rd}$ (kNm)	$M_{\theta,Ed}$ (kNm)	r	$M_{\theta,Rd}$ (kNm)	$M_{\theta,Ed}$ (kNm)	r	ΔM_T (kNm)	e (mm)	$M_{\theta,Ed}$' (kNm)	$M_{\theta,Ed}$' (kNm)	r'
	1	42.18	44.40	1.05	16.37	16.57	1.01	2.22	37.9	42.18	18.79	1.148
θ = 25°	1.5	23.48	24.83	1.058	15.54	14.18	0.912	1.35	23.2	23.48	15.53	0.999
	2	17.93	19.06	1.063	14.76	12.54	0.849	1.13	19.3	17.94	13.66	0.926
	1	50.99	52.78	1.035	14.22	13.19	0.927	1.79	30.6	50.99	14.98	1.053
θ = 15°	1.5	23.54	24.81	1.054	13.00	10.90	0.838	1.28	21.8	23.54	12.18	0.936
	2	16.70	17.85	1.069	12.06	9.37	0.776	1.15	19.7	16.70	10.52	0.872

Note: The ratio r' is defined as $r' = M_{\theta,Ed}'/M_{\theta,Rd}$, where $M_{\theta,Ed}'$ is the moment in the inclined Tee section after redistribution of moment.

Table 10
Geometric and material properties of the test specimens used for validation.

Test	Profile	h (mm)	b_f (mm)	t_f (mm)	t_w (mm)	h_o (mm)	f_y (MPa)
W-1A (Warren [23])	UB 203x133x25	289.8	133.4	7.8	5.8	200	310
W-2A (Warren [23])	UB 203x133x25	309.3	133.4	7.8	5.8	225	320
W-3A (Warren [23])	UB 305x102x25	435	101.6	6.8	5.8	300	350
T-1 (Tsavdaridis [15])	UB 305x165x40	303.4	165.0	10.2	6.0	230	300

Table 11
Comparison of experimental tests (V_{exp}), Enhanced RSM ($V_{E.RSM}$) and Vierendeel bending resistances using the Equivalent Rectangular Opening Method (V_{EqR}).

	No redistribution							With redistribution		
Test	V_{exp} (kN)	M_{exp} (kNm)	V_{EqR} (kN)	V_{EqR}/V_{exp}	$V_{E.RSM}$ (kN)	$M_{E.RSM}$ (kNm)	$V_{E.RSM}/V_{exp}$	$V_{E.RSM}$ (kN)	$M_{E.RSM}$ (kNm)	$V_{E.RSM}/V_{exp}$
W-1A	60	84	52	0.88	54	76	0.90	62	87	1.03
W-2A	56	94	35	0.62	49	82	0.88	57	95	1.02
W-3A	76	132	55	0.73	69	121	0.91	74	130	0.98
T-1	128	38	108	0.84	86	26	0.67	94	28	0.73

Note: The presented total shear force (V) and global moment (M) act at the centreline of the circular web openings that failed in Vierendeel bending.

5. Conclusions

The study shows that Radial Stress Method (RSM) for circular openings in beams may be improved by taking account of the elasto-plastic behaviour of the inclined Tee sections and is more accurate than the Equivalent Rectangular Opening Method. The use of the Enhanced RSM is assessed for a typical cellular beam with large circular openings and subject to constant shear force with varying global moment at the openings and is also compared to 4 beam tests.

The predictions of the Enhanced RSM are compared to results of finite element models using Abaqus starting with first yield around the four sectors of the openings and then with varying levels of post-elastic strain around the openings. The critical angle of the maximum stress is typically at 20° to 25° to the vertical, but this varies with global moment.

The Enhanced RSM shows that the bending resistance of the T-section on the LMS (Q1) of Opening 4 will control the shear force that can be resisted. To develop full plasticity at the HMS and LMS (Q2 and Q1) respectively, a redistribution of moment occurs by a movement in the position of zero moment across the opening. This relatively small redistribution of moment increases the maximum shear force that can be resisted and develops the 4 plastic hinges around the opening corresponding to *Vierendeel* bending failure. The maximum shear force at the opening close to mid-span was found to be 127 kN when using the Enhanced RSM method with a redistribution of moment, compared to the elastic resistance of 73 kN in the most highly stressed quadrant and 111 kN using the equivalent rectangle method.

The elasto-plastic methodology is primarily intended for software development for cellular beams, but the practical benefit is to be able determine accurately the effect of the shear and moment interaction around the 4 quadrants of the openings as a function of the strain that can be developed, dependent on the slenderness of the web outstand. The precise correlation between local buckling of the outstand and edge strain around the opening will be developed in future finite element analyses and physical tests. This will also extend to improvements in the use of the equivalent rectangle method for 'hand' analysis.

The Enhanced RSM is not applicable to polygonal-shaped openings where stress analysis is conceptually different and often simpler. However, the core equilibrium logic of the proposed method can be adapted to other web openings with curved edges by modifying the geometric definitions to ensure that the resulting normal stress is tangential to the opening's edge.

Therefore, future work will include an extensive sensitivity analysis across a wide range of section profiles and web opening sizes for a range of shear and bending combinations. Finally, the geometric and loading conditions leading to yielding in narrow web-posts will be examined and included in the adaptation of the Enhanced RSM method.

CRediT authorship contribution statement

Georgios Psyrras: Writing – original draft, Visualization, Validation, Software, Investigation, Formal analysis, Data curation. **Konstantinos Daniel Tsavdaridis:** Writing – review & editing, Validation, Resources, Project administration, Funding acquisition, Conceptualization. **R. Mark Lawson:** Writing – review & editing, Validation, Supervision, Methodology, Investigation, Conceptualization.

Declaration of competing interest

The authors declare that they have no known competing financial interests or personal relationships that could have appeared to influence the work reported in this paper.

Appendix A. Vierendeel bending resistance of equivalent rectangular opening

Determine the Vierendeel bending resistance for a 337.5 mm diameter opening in the 457 × 152 × 52 kg/m UB, as was used in the FEA, according to the Equivalent Rectangular Opening Method for the following data:

$a_{o,eq} = 0.45 \times 337.5 = 152$ mm.
$h_{o,eq} = 0.9 \times 337.5 = 304$ mm.
$h = 450$ mm.
$h_{T,eq} = (450–304)/2 = 73$ mm.
$b_f = 152$ mm.
$t_f = 10.9$ mm.
$t_w = 7.6$ mm.
$f_y = 355$ N/mm^2.

A.1. Plastic bending resistance of Tee of depth, $h_{T,eq}$

Plastic neutral axis depth from outside of flange:

$$z_{p\ell} = \frac{7.6 \times 62 + 152 \times 10.9}{2 \times 152} = 7.0 \text{ mm}$$

Plastic bending resistance of Tee
$M_{p\ell,T}$ = [7.6 × 62 x (31 + 3.9) + 152 x ($7.0^2 + 3.9^2$)/2] x 355 × 10^{-6} = 7.57 kNm.

A.2. Elastic bending resistance of Tee of depth, $h_{T,eq}$

Elastic neutral axis depth from outside of flange:

$$z_{e\ell} = \frac{152 \times \frac{10.9^2}{2} + 7.6 \times 62 \times 42}{7.6 \times 62 + 152 \times 10.9} = 13.5 \text{ mm}.$$

Inertia of Tee:
$I_T = 152 \times 10.9 \times 8.0^2 + 7.6 \times 62 \times 28.5^2 + 152 \times 10.9^3/12 + 7.6 \times 62^3/12 = 656 \times 10^3$ mm^4.
Elastic bending resistance of Tee
$M_{e\ell,T} = 656 \times 10^3 \times 355$ /(73–13.5) x10^{-6} = 3.91 kNm (=0.52$M_{p\ell,T}$).

A.3. Vierendeel bending resistance of equivalent rectangular opening

Consider firstly the case without interaction of shear and global bending.
Applied Vierendeel bending moment on Tee:
$M_{v,Ed} = V_{Ed}$ x 152 × $10^{-3}/4 = 0.038\ V_{Ed}$
Maximum shear force, $V_{Ed} \leq 7.57/0.038 = 199$ kN.

A.4. Shear resistance of the equivalent depth of the Tee, $h_{T,eq}$

$V_{T,Rd}$ = [7.6 × 62 + 10.9 x (2 × 10.2 + 7.6)/2] x 0.577 × 355 × 10^{-3} = 127.7 kN.
Shear resistance of two T sections, $V_{Rd} = 2 \times 127.7 = 255.4$ kN.
So pure shear does not control but the ratio $V_{Ed}/V_{Rd} = 0.78$.
The effective thickness is reduced to take account of the high shear force acting in combination with Vierendeel bending. The final shear force acting on the Tee is obtained by a process of iteration with the reduced Vierendeel bending resistance, so take $V_{Ed} = 175$ kN as a first iteration. Therefore, $V_{Ed}/V_{Rd} = 175/255.4 = 0.69$.
Reduce the effective thickness of the web for Vierendeel bending according to:
$t_{w,eff} = (1\text{- } (2\ V_{Ed}/V_{Rd}\text{-}1)^2\ t_w = ((1\text{- } (2 \times 0.69\text{–}1)^2) \text{ x } 7.6 = 6.5$ mm.

A.5. Reduced Vierendeel bending resistance of Tee using the effective web thickness, $t_{w,eff}$

Plastic neutral axis depth from outside of flange:

$$z_{p\ell} = \frac{6.5 \times 62 + 152 \times 10.9}{2 \times 152} = 6.8 \text{ mm}$$

Reduced plastic bending resistance of Tee.
$M_{p\ell,T}$ = [6.5 × 62 x (31 + 4.1) + 152 x ($6.8^2 + 4.1^2$)/2] x 355 × 10^{-6} = 6.72 kNm
Maximum shear force, $V_{Ed} \leq 4 \times 6.72/0.152 = 177$ kN.
In a second iteration, the Vierendeel bending resistance is $V_{Ed} \leq 176$ kN.
This shows that the maximum shear force that can be resisted by the opening close to the support (Opening 1) is 176 kN.

A.6. Bending resistance of centre-line of Opening 4 close to mid-span

Area of Tee at centre-line of opening, $A_T = 7.6 \times 45 + 10.9 \times 152 = 1999$ mm^2.
Elastic neutral axis depth of Tee.
$z_e = (152 \times 10.9^2/2 + 7.6 \times 45 \times 33.4)/1999 = 10.2$ mm
Effective depth of section, $h_{eff} = 450\text{–}2 \times 10.2 = 430$ mm (= 0.95 h).
Bending resistance of beam at centre-line of opening,
$M_{Rd} = 1999 \times 430 \times 355$ x $10^{-6} = 305.1$ kNm.
For the opening closest to mid-span at $x = 1.83$ m from support, the bending moment due to a shear force of $V_{Ed} = 176$ kN is:
$M_{Ed} = 176 \times 1.83 = 322$ kNm > 305.1 kNm.
This shows that maximum shear force should be reduced to 167 kN in global bending.

A.7. Modified Vierendeel bending resistance of opening close to mid-span

The axial force in the Tees due to global bending reduces the Vierendeel bending resistance according to:
$M_{T,Rd} = M_{p\ell,T}\ (1\text{- } (N_{T,Ed}/N_{p\ell,T})^2)$

where $N_{T,Ed} = M_{Ed} / h_{eff}$.

This requires a process of iteration by reducing the maximum shear force at the opening close to the point of maximum moment. A reduction in the shear force increases the effective web thickness, which modifies the Vierendeel bending resistance.

Reduce the maximum shear force acting on the opening close to mid-span to $V_{Ed} = 111$ kN.

Therefore, $V_{Ed}/V_{Rd} = 111/255.4 = 0.43 < 0.5$ – no reduction in t_w.

Bending moment on beam at opening, $M_{Ed} = 111 \times 1.83 = 203$ kNm < 305 kNm.

Axial force in Tee, $N_{T,Ed} = 203 \times 10^3 / 430 = 472$ kN.

Axial resistance of Tee, $N_{p\ell,T} = 1999 \times 355 \times 10^{-3} = 710$ kN.

Reduced Vierendeel bending resistance of the Tee is:

$M_{T,Rd} = 7.57$ x $(1- (472/710)^2) = 4.22$ kNm

Maximum shear force, $V_{Ed} \leq 4 \times 4.22/0.152 = 111$ kN.

This shows that the maximum shear force at Opening 4 closest to mid-span is limited to 111 kN by combination of Vierendeel bending with high global bending moment.

Data availability

No data was used for the research described in the article.

References

[1] M.D. Altifillisch, B.R. Cooke, A.A. Toprac, An investigation of open web expanded beams, Welding Res. 22 (2) (1957).

[2] R.G. Redwood, J.O. McCutcheon, Beam tests with unreinforced web openings, J. Struct. Div. 94 (1) (1968) 1–17.

[3] J.K. Ward, Design of composite and non-composite cellular beams, in: SCI Publication 100, 1990.

[4] R.G. Redwood, Design of Beams with Web Holes, Canadian Steel Industries Construction Council, 1973.

[5] H.C. Olander, A method for calculating stresses in rigid frame corners, in: Proceedings of the American Society of Civil Engineers, ASCE, 1953, pp. 1–21.

[6] P. Sahmel, The design, construction and approximate analysis of weld beams and torsion members having large web openings, Schweissen und Schneiden 21 (3) (1969) 116–122.

[7] W.R. Osgood, A theory of flexure for beams with nonparallel extreme fibers, J. Appl. Mech. 6 (3) (1939) 122–126. Available at: https://doi.org/10.1115/1.4008945.

[8] O.W. Blodgett, Design of Welded Structures, James F. Lincoln Arc Welding Foundation, Cleveland, 1966.

[9] J.R. Yost, et al., Experimental and analytical investigation of service-load stresses in cellular beams, J. Eng. Mech. 138 (8) (2012), https://doi.org/10.1061/(asce)em.1943-7889.0000405. Available at.

[10] R.M. Lawson, A. Basta, A. Uzzaman, Design of stainless steel sections with circular openings in shear, J. Construct. Steel Res. 112 (2015), https://doi.org/10.1016/j.jcsr.2015.04.017. Available at.

[11] British Standards Institution, Eurocode 3: Design of Steel Structures – Part 1–13: Beams with Large Web Openings, 2024. BS EN 1993-1-13:2024.

[12] K.F. Chung, T.C.H. Liu, A.C.H. Ko, Investigation on Vierendeel mechanism in steel beams with circular web openings, J. Construct. Steel Res. 57 (5) (2001), https://doi.org/10.1016/S0143-974X(00)00035-3. Available at.

[13] K.F. Chung, C.H. Liu, A.C.H. Ko, Steel beams with large web openings of various shapes and sizes: an empirical design method using a generalised moment-shear interaction curve, J. Construct. Steel Res. 59 (9) (2003), https://doi.org/10.1016/S0143-974X(03)00029-4. Available at.

[14] K.D. Tsavdaridis, C. D'Mello, Vierendeel bending study of perforated steel beams with various novel web opening shapes through nonlinear finite-element analyses, J. Struct. Eng. 138 (10) (2012), https://doi.org/10.1061/(asce)st.1943-541x.0000562. Available at.

[15] K.D. Tsavdaridis, C. D'Mello, Optimisation of novel elliptically-based web opening shapes of perforated steel beams, J. Construct. Steel Res. 76 (2012), https://doi.org/10.1016/j.jcsr.2012.03.026. Available at.

[16] K.D. Tsavdaridis, C. D'Mello, M. Hawes, Experimental study of ultra shallow floor beams (USFB) with perforated steel sections, in: The 11th Nordic Steel Construction Conference 2009 (NSCC 2009). 2-4 September 2009, Malmö, Sweden, Reference no: 128, 2009, pp. 312–319.

[17] P. Panedpojaman, T. Thepchatri, S. Limkatanyu, Novel simplified equations for Vierendeel design of beams with (elongated) circular openings, J. Construct. Steel Res. 112 (2015), https://doi.org/10.1016/j.jcsr.2015.04.007. Available at.

[18] R.M. Lawson, M. Stergiopoulos, M. Rowell, Design of cold formed section beams with elongated circular openings based on tests, Thin Walled Struct. 204 (2024) 112256.

[19] Dassault Systèmes, Abaqus/CAE 2020, Available at: https://www.3ds.com/products-services/simulia/products/abaqus/.', 2020.

[20] Dassault Systèmes, Abaqus 2020 Reference Library, Available at: https://help.3ds.com/2020x/.', 2020.

[21] X. Yun, L. Gardner, Stress-strain curves for hot-rolled steels, J. Constr. Steel Res. 133 (2017) 36–46. Available at: https://doi.org/10.1016/J.JCSR.2017.01.024.

[22] British Standards Institution, Eurocode 3: Design of Steel Structures – Part 1–1: General Rules and Rules for Buildings, 2005. BS EN 1993-1-1:2006.

[23] J. Warren, Ultimate Load and Deflection Behaviour of Cellular Beams, University of Natal, 2001. Available at, https://researchspace.ukzn.ac.za/items/bbc36ad9-3d4c-4db9-a2ad-7532e347a950.